Desalination and Water Treatment
www.deswater.com

doi: 10.5004/dwt.2018.22806

126 (2018) 333–344
September

Facile synthesis of pH-sensitive carboxymethyl chitosan and its tunable adsorption property toward anionic and cationic dyes

Min Wu, Yunshan Bai*, Wenyun Li, Dandan Xu, Wenjuan Chen, Hongzhu Ma*

School of Chemistry and Chemical Engineering, Shaanxi Normal University, Xi'an, Shaanxi 710119, China, Tel. +86 29 81530726; Fax: +86 29 81530727; emails: baiys@snnu.edu.cn (Y. Bai), hzmachem@snnu.edu.cn (H. Ma)

Received 1 March 2018; Accepted 13 July 2018

ABSTRACT

N,O-carboxymethyl chitosan (CCS_x) adsorbents with tunable adsorption and separation capacity were successfully prepared by chitosan (CS) and monochloroacetic acid (MCA) with various amounts. The structures and compositions were characterized by Fourier-transform infrared spectroscopy, scanning electron microscopy, X-ray powder diffraction, zeta potential, thermogravimetric analysis, and N_2 adsorption–desorption isotherm. Results showed that carboxymethylation of CS with MCA occurred mainly at C_6–OH and C_2–NH_2 positions. The pH-sensitive and tunable adsorption capacities toward various dyes were studied and optimized. At the optimal pHs (pH ≥ 5 for methylene blue (MB) and pH ≤ 3 for methyl orange (MO)), the highest removal efficiencies of 94.5% and 90.6% for MB and MO, respectively, were observed for CCS_1. The adsorption isotherm data better fitted with Langmuir model ($R^2 > 0.99$), and the maximum adsorption capacity of 64.56 and 92.51 mg g^{-1} were obtained for MB and MO, respectively. The kinetics of adsorption was described by the pseudo-second-order model. The regeneration study showed that the percentage uptake declined slightly for MO after five cycles. Moreover, MB or MO can be separated efficiently at pH ≥ 5 or pH ≤ 3 in the MB/MO binary system, indicating its selective adsorption and separation property, especially its potential application in practical wastewater treatment.

Keywords: Carboxymethyl chitosan; pH sensitive; Tunable adsorption; Dyes

1. Introduction

With the increasing concern on environment protection in recent years, removal of pollutants has gradually attracted more and more attention. Dyes, the main pollutant, are widely used in many industries and produced large amount of dye-containing wastewater [1]. Lots of them are toxic and hazardous to aquatic organisms; however, it is hard to be treated because of the complex aromatic molecular structures [2]. Thus, removal of dyes from wastewater becomes a significant issue. Various techniques, such as electrochemical oxidation, biological treatment, precipitation, flocculation, ion exchange, reverse osmosis, and adsorption, have been applied for effluents treatment [3]. Among them, adsorption has been the most competitive and extensively used process owing to the economy, convenience, and high efficiency.

Nowadays, various facile absorbents have been used for the removal of dyes. A cost-effective and eco-friendly activated carbon prepared by microwave-assisted chemical activation was used for the removal of anionic dye (CR) [4]. The brown macroalga can act as a promising adsorbent for the removal of methylene blue (MB) [5]. Albadarin et al. [6] synthesized activated lignin–chitosan extruded pellets for MB adsorption, and the maximum adsorption capacity was 36.25 mg g^{-1}. Trisodium citrate-based magnetite nanocomposite (Fe_3O_4–TSC) was used for MG removal, and the adsorbent can be effortlessly separated from mixed solutions

* Corresponding authors.

using an external magnetic field [7]. Other adsorbents, such as guar gum/Al_2O_3 nanocomposite [8], polyaniline Zr(IV) selenotungstophosphate nanocomposite [9], amberlite Ira-938 resin [10], potassium hydroxide-treated palm kernel shell [11], and ZrO_2/Fe_3O_4/chitosan (CS) nanomaterials [12] have also been reported to be used as promising adsorbents for dye removal from textile wastewater.

Among these adsorbents, natural polymers like CS, starch, and cellulose are receiving increasing attention due to the presence of reactive hydroxyl, amino, and carboxyl groups [13]. CS, as a well-known natural aminopolysaccharide with high binding capacity, wide availability, and high molecular weight, is widely studied and applied because of its non-toxic and biodegradable properties [14]. Some authors have shown that CS is well recognized for dyes and heavy metals removal and its efficient adsorption potential can be attributed to large number of functional groups [15,16]. However, the application of CS is hindered because of its low surface area, low mechanic resistance, and inefficiency for cationic dyes removal [1,17].

To overcome these weaknesses, CS is often modified with functional groups (–COOH, –SO_3H) on its side chains to improve its adsorption capacity toward cationic dyes. These functional groups are pH sensitive and may display different forms in acid and alkaline conditions, thus causing different adsorption property [18]. Xu et al. [19] has functionalized CS beads with citric acid for effective adsorption of positively charged lysozyme with 42.1 mg g^{-1} adsorption capacity within 3 h. Yang et al. [20] has prepared polyurethane foam membrane filled with humic acid-CS crosslinked gels through ionic crosslinking between carboxyl and protonated amino groups for dye removal. It can separate MB effectively from methyl orange (MO)/MB and simultaneously remove RB and MB from RB/MB solution by adjusting the dosage of HA [20]. However, limited research on the tunable selective adsorption property of CS was reported.

CS modified with functional groups can provide additional adsorption sites. Meanwhile, amino groups and carboxyl groups exhibited different forms at various pHs, thus with tunable adsorption capacity. For this purpose, the objective of this work is to fabricate pH-sensitive amphiphilic adsorbent material based on CS with selective adsorption capacity toward the cationic and anionic dyes. Carboxymethylation of CS by various amounts of monochloroacetic acid (MCA) (MCA/CS = 0, 0.5, 1.0, 1.5, and 2.0 in mass ratio) with more cationic adsorption sites and tunable adsorption capacity was synthesized and characterized by Fourier-transform infrared spectroscopy (FT-IR), scanning electron microscopy (SEM), X-ray powder diffraction (XRD), Zeta potential measurements, thermogravimetric analysis (TGA), and N_2 adsorption–desorption isotherm. The tunable selective adsorption capacity toward the cationic or anionic dye was studied. The adsorption behaviors of carboxymethyl chitosan (CCS_1) were systematically investigated by the selective adsorption, adsorption isotherms, and kinetics, and the possible adsorption mechanism was also proposed.

2. Experimental section

2.1. Materials

CS $(C_6H_{11}NO_4)_n$ with molecular weight of 1×10^5 (>90% degree of deacetylation) was purchased from Xi'an Golden-Shell Biochemical Co., Ltd. (China). MCA (A.R.), sodium hydroxide (NaOH, A.R.), ethanol (CH_3CH_2OH, A.R.), isopropyl alcohol (C_3H_8O, A.R.), MB ($C_{16}H_{18}ClN_3S{\cdot}3H_2O$, A.R.) and MO ($C_{14}H_{14}N_3NaO_3S$, A.R.), and hydrochloric acid (HCl, 36%–38%) were obtained from Sinopharm Chemical Reagent Co., Ltd. (Xi'an, Shaanxi Province) and used directly without further purification.

2.2. Synthesis of pH-sensitive CCS_x adsorbents

The CCS_x adsorbents were prepared according to the reference reported [21,22]. Typically, 1 g of CS was scattered in 50 mL of NaOH solution (1.35 g of NaOH dissolved into 60% (V/V) isopropyl alcohol solution) and alkalified for 1 h at 40°C. Then, a certain amount of MCA (MCA/CS = 0, 0.5, 1.0, 1.5, and 2.0 in mass ratio) dissolved in 20 mL of isopropyl alcohol was introduced and reacted for 4 h at 40°C, stood for 10 min, separated the white precipitation and distributed it into 20 mL of ethanol, regulated pH to 7 with hydrochloric acid, extracted the solid powder and dried at room temperature, and obtained the amphiphilic adsorbent, denoted as CCS_x (x = 0, 0.5, 1.0, 1.5, and 2.0).

The deacetylation degree (DD) of CS and the degree of carboxymethyl substitution (DS) of CCS_x were calculated using elemental analysis data according to the change of C/N ratio before and after the introduction of carboxymethyl groups by Eqs. (1) and (2) [23,24]:

$$\mathrm{DD}(\%) = \left(1 - \frac{\mathrm{C}\%/\mathrm{N}\% - 5.145}{6.816 - 5.145}\right) \times 100 \quad (1)$$

$$\mathrm{DS}(\%) = [7/12 \times (\mathrm{C}\%/\mathrm{N}\%) + \mathrm{DD} - 4] \times 100 \quad (2)$$

2.3. Characterization of CCS_x adsorbents

The changes of functional carboxymethyl group of CS were observed by FT-IR (Tensor 27, Bruker, Germany) at room temperature in the range of 4,000–400 cm^{-1} using KBr pellets.

The crystal structures and compositions of various CCS_x samples were measured by powder XRD patterns with Rigaku Corporation XRD/Max2550VB+/PC and recorded in the range of 2°–80° with a scanning rate of 0.02° s^{-1}.

The surface morphologies and the elemental compositions of the various adsorbents were determined by SEM and energy dispersive spectroscopy (EDX; Quanta 200, FEI, USA).

Zeta potentials of the samples were determined using a micro-electrophoresis meter (ZEN3690, Malvern). A certain amount of the adsorbents was dispersed in distilled water with the initial solution pH ranging from 2.0 to 11.0 by adjustment using 0.1 mol L^{-1} of NaOH or HCl solution.

TGA was conducted on a thermoanalyzer system (USA) at a heating rate of 10°C min^{-1} from 25°C to 800°C with samples of 4–10 mg.

The Brunauer–Emmett–Teller (BET) specific surface areas and pore structures of adsorbents were obtained from nitrogen adsorption–desorption data using a BET ASAP2020 Mike (USA).

2.4. The adsorption experiments in single-dye system

The cationic dye MB and anionic dye MO, frequently used in the real printing and dyeing industry, were selected as the model dye pollutants to investigate the various adsorption performance of CCS_x. All the experiments were performed with the simulated solution prepared by dissolving a precise amount of MB or MO in deionized water.

For the adsorption experiments in single-dye system, 0.02 g of CCS_x was added into 10 mL 50 mg L^{-1} of MB or MO with stirring at room temperature, adjusted the pH of the solution with 0.1 mol L^{-1} of NaOH or HCl and monitored by pH meter (PHS-3C, Shanghai Yielectric Science Co., Ltd., China).

After a certain time interval, the adsorbent was isolated by centrifugation at 800 rpm for 2 min. The residual dye was then tested by measuring the absorbance of the solution at λ_{max} (465 nm for MO and 664 nm for MB), using a UV–Vis spectrophotometer (UVT6, Beijing Purkinje General Instrument Co., Ltd., China). The color removal (R%) of MO or MB and adsorption amount (q_t) were calculated according to Eqs. (3) and (4):

$$R(\%) = \frac{(C_0 - C_t)}{C_0} \times 100\% \quad (3)$$

$$q_t = \frac{(C_0 - C_t)V}{W} \quad (4)$$

where C_0 and C_t (mg L^{-1}) are the respective MO or MB concentration in solution at initial time and at time t (min); q_t (mg g^{-1}) is the amount of MO or MB adsorbed onto CCS_x at time t; V (mL) is the volume of MO or MB solution; and W (mg) is the mass of CCS_x. All experiments were repeated three times, and the average data and error bars were calculated and presented.

2.5. The selective adsorption process in MO/MB binary system

The MO and MB (50 mg L^{-1} of MO and 50 mg L^{-1} of MB) binary solution was selected as the representative complex system to further study the selective adsorption property of CCS_1. In total, 0.02 g of CCS_1 was added into MO/MB mixture at various pH values. The absorbances of dyes before and after adsorption were also detected by UV-Vis spectroscopy.

2.6. Regeneration and recycle of CCS_1

A total of 0.02 g CCS_1 was introduced into 10 mL 50 mg L^{-1} of MB or MO solution with stirring at 25°C for 10 min. After that, the dispersion system was centrifuged at 800 rpm for 2 min. Separated the adsorbed adsorbent and 10 mL ethanol (adjusted pH = 11 or 3 by 0.1 mol L^{-1} of NaOH or 0.1 mol L^{-1} of HCl) was added with stirring for 30 min for desorption. Then the regenerated adsorbent was dried for the next cycle.

3. Results and discussion

3.1. Carboxymethylation of CS

The reactive sites of CS molecules, C_2–NH_2, C_3–OH, and C_6–OH all have strong reactivity and can take place carboxymethylation reaction in theory. So, selective substitution site for N- versus O-CCS occur. According to the references reported [25,26], the substituted reaction is difficult at C_3–OH because of the steric effect and the intermolecular hydrogen bonding interaction between C_3–OH and partial C_2–NH_2. The carboxymethylation at C_6–OH is always superior to C_2–NH_2. However, when the reaction temperature was above 20°C, the substitution of the carboxymethyl preferentially occurred on the –OH groups in the water/isopropyl alcohol solvent mixture. The activity of C_6–OH decreased and C_2–NH_2 increased with increasing water content in the solvent [27]. Carboxymethylation can take place between pretreated CS by alkaline with chloroacetic acid in the presence of isopropanol [28]. Alkali infiltrate in the chain of CS, swell, and transform the hydroxyl and amino into sodium salt that was beneficial for etherification of CS to obtain N,O-CCS. The whole process can be depicted in Fig. 1.

3.2. Characterization of the adsorbents

The FT-IR spectroscopy is applied to explain the changes in chemical structures and the functional groups of the samples [29], and the results are shown in Fig. 2(a). The broad band at 3,440–3,445 cm^{-1} was assigned to –OH and –NH stretching vibrations. Band due to the stretching vibrations of C–H bond was observed at 2,876 cm^{-1} [30]. The band at 1,657 cm^{-1} was assigned to the residual acetamido groups that remained after deacetylation of chitin during the production process of CS. The N–H bending vibration of terminated amine in CS was observed at 1,596 cm^{-1} [31]. The band at 1,380 cm^{-1} derived from the primary amine of CS [32]. The peaks at 1,427 cm^{-1}, 1,157 cm^{-1}, 1,087 cm^{-1}, and 1,058 cm^{-1} were attributed to the C–N axial deformation (–NH_2 band), special (1-4)-glucosidic band in polysaccharide unit, stretching vibration of C–O–C in the glucose circle, and stretching vibration of C–O from the primary alcohol in CS, respectively [32,33].

After carboxymethylation, similar spectra of CCS_x adsorbents were detected, indicating that similar chemical reaction occurred in the carboxymethylation process. The broad band

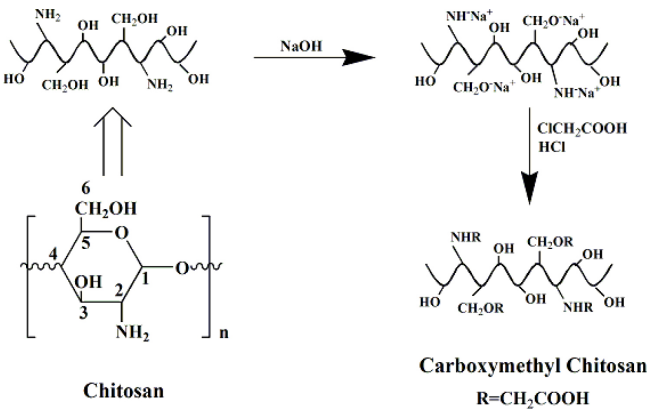

Fig. 1. Synthesis of N-, O-carboxymethyl chitosan.

near 3,440 cm^{-1} corresponding to the stretching vibrations of the O–H and N–H groups of CS, shifted to lower frequencies and weakened. The peaks at 1,657 and 1,596 cm^{-1} overlapped and the shoulder absorption peak of 1,597 cm^{-1} corresponded to the asymmetric stretching vibrations of the carboxylate ions and the N–H bending vibrations [21]. The band at 1,427 cm^{-1} strengthened and shifted to 1,423 cm^{-1} which was caused by symmetric stretching vibration of functional groups of COO^-. The peak at 1,058 cm^{-1} strengthened gradually, indicating that carboxymethylation happened on C_6–OH. These observations indicated the carboxymethylation carried out simultaneously and partly on C_2–NH_2 and C_6–OH position, which was consistent with the reference reported [21,34].

Fig. 2(b) displays the X-ray diffractogram of various adsorbents. Two characteristic diffraction peaks of the native CS displayed at about 2θ = 10.52° and 20.07°, which are attributed to intramolecular hydrogen bonding, and the existence of an amorphous structure related to mixture of (001) and (100), and (101) and (002), respectively [35,36]. After carboxymethylation, the intensities of these peaks dramatically decreased with increasing of the degree of carboxymethyl substitution of CCS_x. These observations indicated that this carboxymethylation process weakened the CS intramolecular or intermolecular hydrogen bonds. The introduction of polar group (–CH_2COOH) decreased the amorphous state of CS, and increased its adsorption capacity.

As TGA curves (Fig. 2(c)) shown, three weight loss stages were observed for all CS samples. The first stage with a weight loss about 10% at less than 100°C, related to the loss of physical adsorption of water on the adsorbent surface. The second stage about 39% weight loss in the range of 250°C–350°C, assigned to the degradation and deacetylation of functional groups of CS. The third stage at 350°C–800°C with a mass loss of 17.0% related to the degradation of ring residues [37]. Similar thermal stability was observed for all CCS_x that was benefit for the practical application.

Zeta potential is the characteristics of an adsorbent that affects the interaction and the adsorption capacity. As can be seen in Fig. 2(d), various zeta potentials of CS, CCS_1, and $CCS_{1.5}$ from +60 to –50 mV were observed at pH range of 2–11, revealing the different surface properties of CCS_x adsorbent. It is well acknowledged that when the pH value of the solution is lower than pH of zero point charge (pH_{zpc}), the adsorbent surface is positively charged due to the protonated $–NH_3^+$ and $–OH_2^+$ groups. The lower the pH value of the solution, the more favorable of anionic dyes

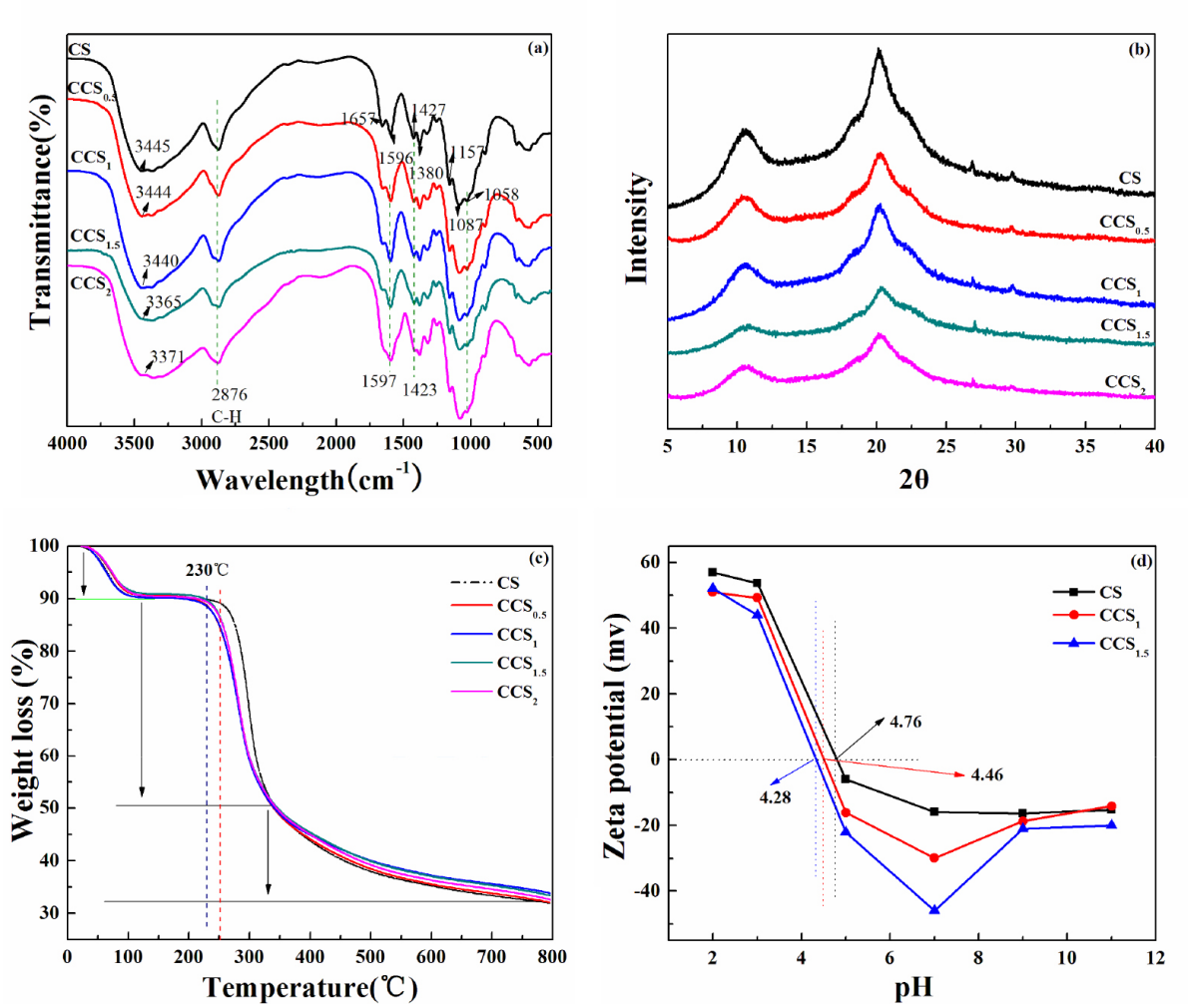

Fig. 2. (a) FT-IR spectra, (b) XRD, (c) TGA curves, and (d) zeta potentials of CCS_x.

adsorption. When the pH value of the solution is higher than pH_{zpc}, negatively charged surface of the adsorbent is due to deprotonation of carboxyl groups and hydroxyl groups. For CCS_1 and $CCS_{1.5}$, pH_{zpc} shifted from 4.76 (CS) to lower values of 4.46 and 4.28, respectively, indicating more carboxymethyl groups were introduced during the carboxymethylation of CS, thus leading to more negative charge of $CCS_{1.5}$ [38].

SEM images of CS, CCS_1, CCS_1-MO, and CCS_1-MB are illustrated in Fig. 3. A long thin crystal with a smooth and homogeneous surface was detected for CS, whereas small cracks, rough and irregular surface was observed for CCS_1, indicating the functional groups were well integrated onto the surface [39]. After adsorption, micropores and light roughness could be found, indicating the effective adsorption capacity of CCS_1.

The elemental analyses of CS and CCS_x were conducted to determine DD and DS, and the results are shown in Table 1. The DS of CCS_x increased with the mass ratios of MCA to CS increasing, thus changing the internal structure and crystalline region of CS, which were consistent with XRD analysis [40].

Specific surface area is an intrinsic property of any porous and powered particle which can divulge crucial information about its adsorption properties [41]. The structural characteristics of the prepared adsorbents are summarized in Table 2. Lower surface areas and pore sizes were observed, indicating that the pore volume and surface area were not the key factor during the adsorption process [42].

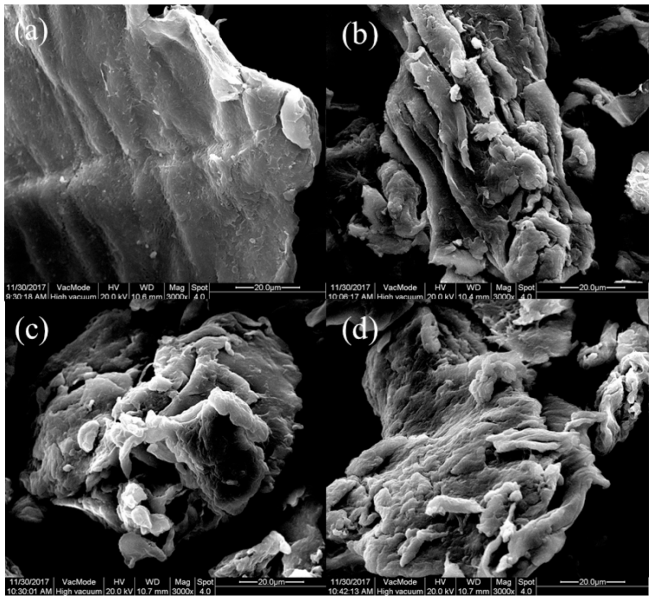

Fig. 3. SEM images of (a) CS, (b) CCS_1, (c) CCS_1-MO, and (d) CCS_1-MB.

3.3. Studies on adsorption capacities of CCS_1

3.3.1. Effect of MCA amounts

The effect of various mass ratios of MCA to CS (0, 0.5, 1.0, 1.5, and 2.0) on MB and MO removal at various pHs were studied. As can be seen from Fig. 4, the adsorption efficiencies of CCS_x were dependent on MCA amounts and/or pH values. The color removal of MB increased, while MO removal decreased with the increase of MCA dosage, moreover, MO removal decreased and MB removal increased dramatically at pH > 3, indicating that adsorption capacities of the adsorbent CCS_x were pH sensitive and tunable just by changing the mass ratio of MCA/CS. When the dosage of MCA increased to 1:1, MB removal reached to a high value (94.5%) and then changed slightly with increasing dosage of MCA, indicating further increasing MCA dosage contributed negligible to the improvement of adsorption capacity of CCS_x toward cationic dye. However, the removal of MO was mainly supervised by the initial pH of the solution and prohibited significantly by the introduction of MCA at pH > 5. The removal of MO decreased obviously from 94.7% to 68.1% with MCA dosage increasing from 0:1 to 2:1 at pH 3, further confirming that the pH dependence and tunable adsorption properties of CCS_x adsorbent toward cationic and anionic dyes.

3.3.2. Effect of initial pH

The pH of solution is one of the most important parameters that determined the removal percentages and adsorption capacity of the adsorbents. The experiments were carried out in pH range of 2–11, and the results are illustrated in Fig. 5. It was observed that the removal of MO decreased from 90.6% to 1.5% with pH increasing from 2 to 11, while MB removal

Table 2
Surface parameters of CS and CCS_1

Adsorbents	S_{BET} ($m^2\ g^{-1}$)	Pore volume ($cm^3\ g^{-1}$)
CS	0.0453	0.000827
CCS_1	0.0382	0.000941

Table 1
EDX results of CS and CCS_x and the degree of substitution

Samples	C (wt. %)	N (wt. %)	C/N	DD (%)	DS (%)
CS	53.22	10.16	5.24	94.3	–
$CCS_{0.5}$	63.00	11.58	5.44	–	11.6
CCS_1	61.96	10.73	5.77	–	30.9
$CCS_{1.5}$	59.00	10.03	5.88	–	37.3
CCS_2	61.48	10.17	6.04	–	46.6

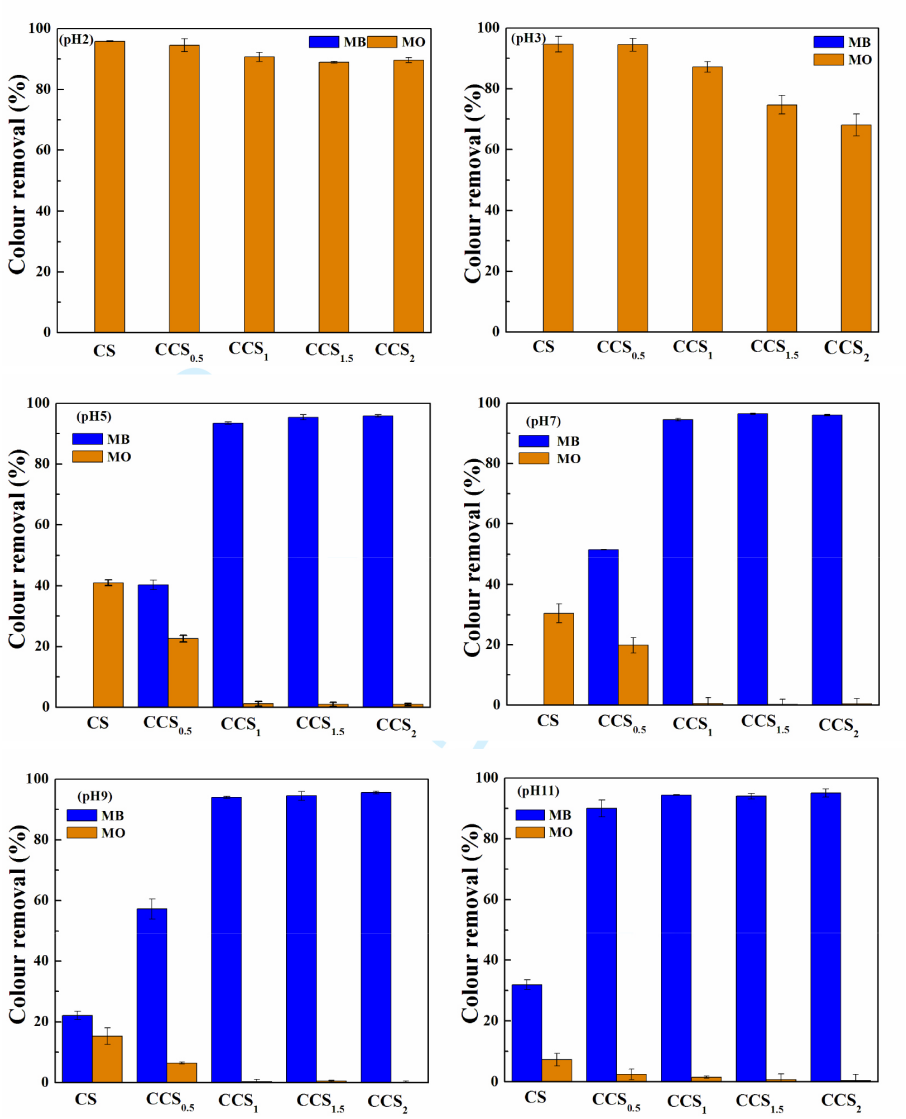

Fig. 4. Effect of MCA amounts on MB and MO removal at various pH values.

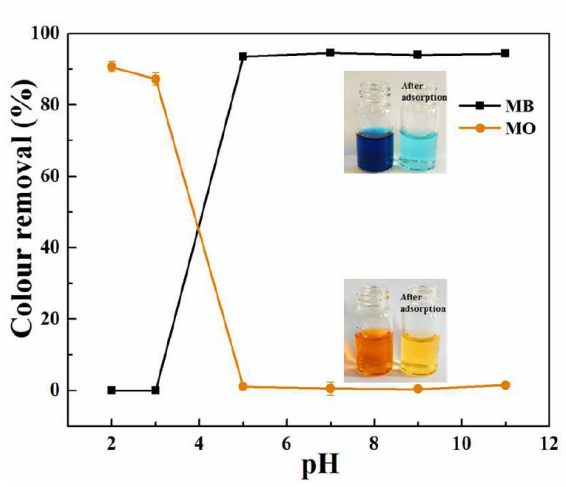

Fig. 5. Effect of pH on dyes removal by CCS_1.

increased from 0% to 94.5%, indicating that the adsorption capacities of adsorbents exhibited pH dependence [43].

For the adsorption process, the cationic functional groups existed in protonated form and the surface of the adsorbent positive charged at pH < pH_{zpc} (4.46 for CCS_1), electrostatic interaction between CCS_1 and dye molecules was dominated: as for cationic dye MB, electrostatic repulsion caused MB removal were almost negligible at strong acid pHs (2–3), while electrostatic attraction resulted in high MO removal (>80%). When pH > pH_{zpc}, MO removal drastically decreased, while MB removal sharply increased with the increase of pH up to 5, then almost unchanged from pH 5 to 11, it was due to the fact that both deprotonated amino and hydroxyl groups led to the negative charged surfaces of the adsorbents, and thus attractive interactions between adsorbent and negative functional groups of MO decreased, and attractive interactions between MB and CCS_1 increased, these phenomenon were also confirmed by Zeta potential test [44,45].

3.3.3. Effect of initial concentration of dyes and adsorption isotherms

The effects of initial concentration of MO and MB on adsorption capacity of CCS_1 were investigated from 50 to 300 mg L^{-1} at pH = 3 and neutral conditions, respectively (Figs. 6(a) and 6(b)). It was observed that as the initial concentration of MB and MO increased to 200 mg L^{-1}, the adsorption amount of dyes increased and gradually reached the equilibrium at 10 min (87.28 and 60.85 mg g^{-1} for MB and MO, respectively). This might be due to the fact that large numbers of vacant active sites were available for the adsorption of dye molecules at lower initial concentration. When the effective adsorption sites of adsorbent were gradually occupied and saturated, it was difficult to capture more additional dye molecules, so the adsorption capacity of the adsorbent will not increase with the increase of the dye concentration, and the adsorption reach saturated [46]. Meanwhile, the aggregation of dyes molecules diffused uneasily into the inner structure of CCS_1 adsorbent and more dyes molecules were left in the solution at high concentration, thus leading to a slight decrease in color removal [47].

In order to describe better the adsorbent behavior, two isothermal adsorption models (Langmuir and Freundlich) were used for linear fitting of the experimental data (Figs. 6(c) and 6(d)). The related parameters and error functions [48] are shown in Table 3.

The Langmuir and Freundlich models in linear form can be represented as follows:

$$\frac{C_e}{q_e} = \frac{1}{K_L q_m} + \frac{C_e}{q_m} \tag{5}$$

$$\ln q_e = \ln K_F + \frac{1}{n} \ln C_e \tag{6}$$

where C_e (mg L^{-1}) is the equilibrium concentration of MB or MO in solution (mg L^{-1}); q_e (mg g^{-1}) is the amount of MB or MO adsorbed per unit weight of adsorbents at equilibrium; q_m (mg g^{-1}) is the maximum adsorption capacity; K_L (L mg^{-1}) is the equilibrium constant of Langmuir equation related to the adsorption free energy; and K_F and n are the Freundlich constants related to the adsorption capacity and intensity.

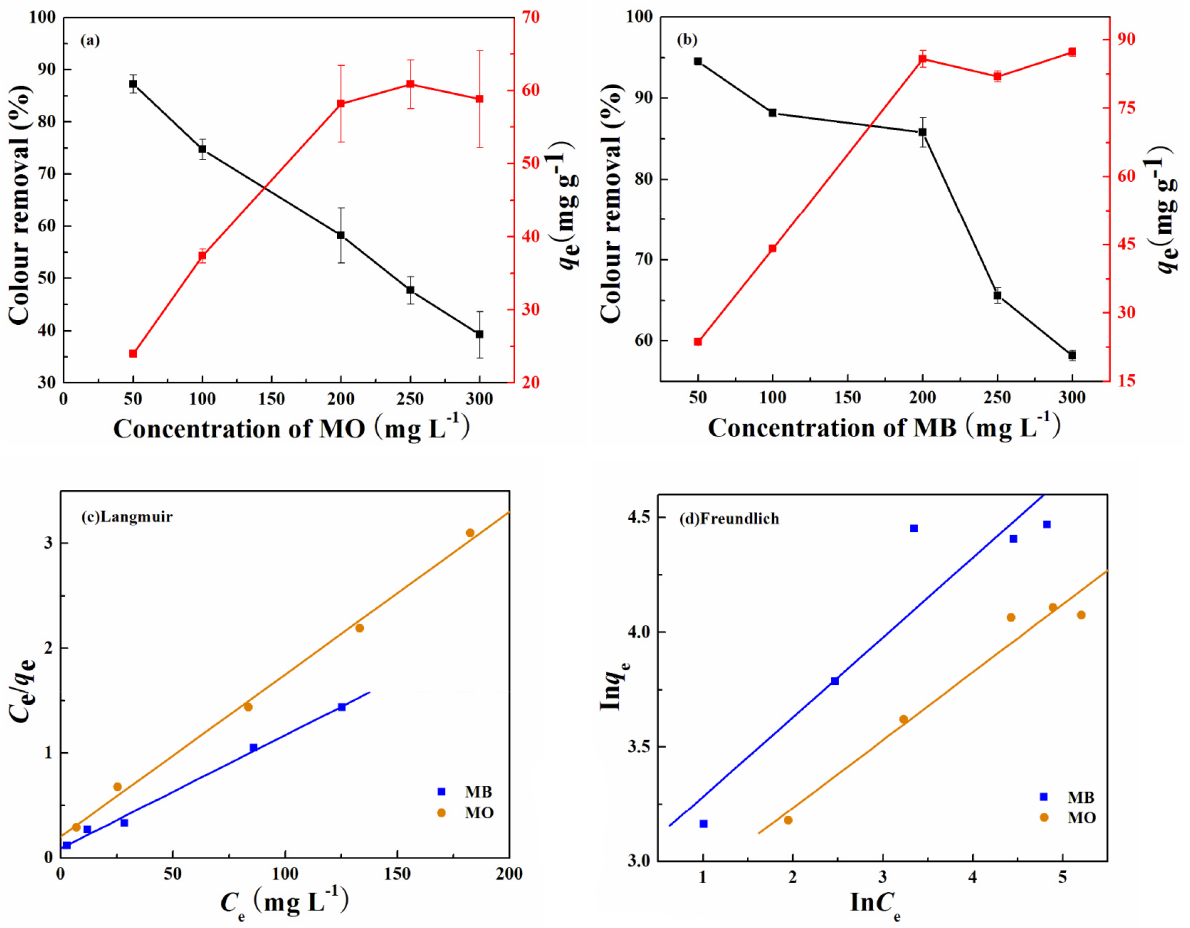

Fig. 6. Effects of initial concentration of (a) MO and (b) MB on the color removal and the linear fitting curves of (c) Langmui and (d) Freundlich equation.

The correlation coefficient R^2 and other error functions of Langmuir model were much closer to 1 or lower than those of Freundlich, respectively, indicating that the Langmuir model described the adsorption process better (Table 3). Moreover, the maximum adsorption capacities (q_m) of CCS_1 (92.51 and 64.56 mg g^{-1} for MB and MO, respectively) calculated by Langmuir model were closer to the experimental results. Therefore, the adsorption could be described better by the Langmuir model and it was driven by the monolayer formation [49].

The maximum adsorption capabilities of other adsorbents reported in previous studies are summarized and compared with CCS_1 (Table 4). CCS_1 exhibited relative higher adsorption capacity and lower cost, which should be act as a promising adsorbent for the removal of dyes in wastewater treatment.

3.3.4. Adsorption kinetics

To investigate the adsorption mechanism, the well-known pseudo-first-order and pseudo-second-order kinetic models were fitted to the adsorption data, using the following equations [7,53]:

$$\ln(q_e - q_t) = \ln q_e - k_1 t \tag{7}$$

$$\frac{t}{q_t} = \frac{1}{K_2 q_e^2} + \frac{1}{q_e} t \tag{8}$$

where q_e and q_t (mg g^{-1}) are the amounts of MB or MO adsorbed onto CCS_1 at equilibrium and at time t, respectively. k_1 (min^{-1}) and k_2 (g mg^{-1} min^{-1}) are the adsorption rate constants of pseudo-first-order and pseudo-second-order models.

The pseudo-first-order and pseudo-second-order kinetic curves, the values of different constant parameters and correlation coefficients are given in Fig. 7 and Table 5. It was observed that higher correlation coefficients (R^2) of pseudo-second-order model of 0.9900, 0.9781 for MB and MO, were obtained. Moreover, much lower other error functions values were calculated by the pseudo-second-order kinetics, suggesting the pseudo-second order model described better the adsorption process and chemisorptions involved in the sorption process [48].

3.4. Selective adsorption and separation performance of CCS_1 in co-existed mixed dyestuffs

The binary system of anionic dye MO and cationic dye MB in acid (pH = 3) and neutral (pH = 7) were chosen to explore the selective adsorption performance of CCS_1 (Fig. 8). At acidic condition (pH = 3), MO could be adsorbed effectively and MB adsorption was suppressed absolutely. While at neutral condition (pH = 7), the situation was completely on the contrary: MB could be selectively adsorbed and MO hardly adsorbed. These results were consistent with the effect of initial pH of the solution in the single dye system, indicating CCS_1 can

Table 3
Langmuir and Freundlich isotherm parameters and error functions

	$q_{e,exp}$ (mg g^{-1})		Kinetics parameters	R^2	X^2	SSE	SAE	ARE	MPSD	HYBRID
MB	87.28	Langmuir	q_m = 92.51 mg g^{-1} k_L = 0.1199 L mg^{-1}	0.9940	4.8516	313.7087	28.0789	9.0619	16.6340	160.8101
		Freundlich	n = 2.88 k_F = 18.85	0.8736	13.4906	889.1411	49.2048	15.1635	21.3596	355.1481
MO	60.85	Langmuir	q_m = 64.56 mg g^{-1} k_L = 0.0765 Lmg^{-1}	0.9957	0.8934	40.1236	12.1095	5.4049	9.1775	32.6399
		Freundlich	n = 3.38 k_F = 14.04	0.9595	1.9467	97.0929	18.3414	8.0571	13.1027	67.4865

Table 4
Comparison of the adsorption capacities of various adsorbents

Adsorbents	MO q_m (mg g^{-1})	MB q_m (mg g^{-1})	Refs
Oxygen functionalized carbon nanocomposites	–	215.28	[50]
Microporous chitosan monoliths doped with graphene oxide	567.07	–	[47]
Polyurethane membrane filled with UiO-66-NH_2 Nanoparticles	–	0.91	[51]
PCN-222(MOFs)	589	906	[52]
Carboxymethyl chitosan-modified magnetic-cored dendrimers	20.85	96.31	[21]
Polyurethane foams membrane filled with HA-CS	13.51	10.31	[20]
CCS_1	92.51	64.56	This paper

Table 5
Kinetics parameters and error functions

Dyes	MB		MO	
	Pseudo first order	Pseudo second order	Pseudo first order	Pseudo second order
Kinetics parameters	$q_{e,1}$ = 7.19 mg g^{-1} k_1 = 0.1767min^{-1}	$q_{e,2}$ = 25.44 mg g^{-1} k_2 = 0.0323 g mg^{-1} min^{-1}	$q_{e,1}$ = 3.27 mg g^{-1} k_1 = 0.0515min^{-1}	$q_{e,2}$ = 22.15 mg g^{-1} k_2 = 0.4773 g mg^{-1} min^{-1}
R^2	0.6690	0.9900	0.0649	0.9781
X^2	277.4218	0.5281	3,502.7875	2.3142
SSE	1,303.2668	9.2332	1,756.4948	49.3749
SAE	79.8079	5.9715	93.0762	11.3836
ARE	358.7977	6.3084	4,127.3729	10.5911
MPSD	99.8724	11.5437	123.6634	25.7227
HYBRID	2,042.9307	19.7511	2,968.1465	103.8327

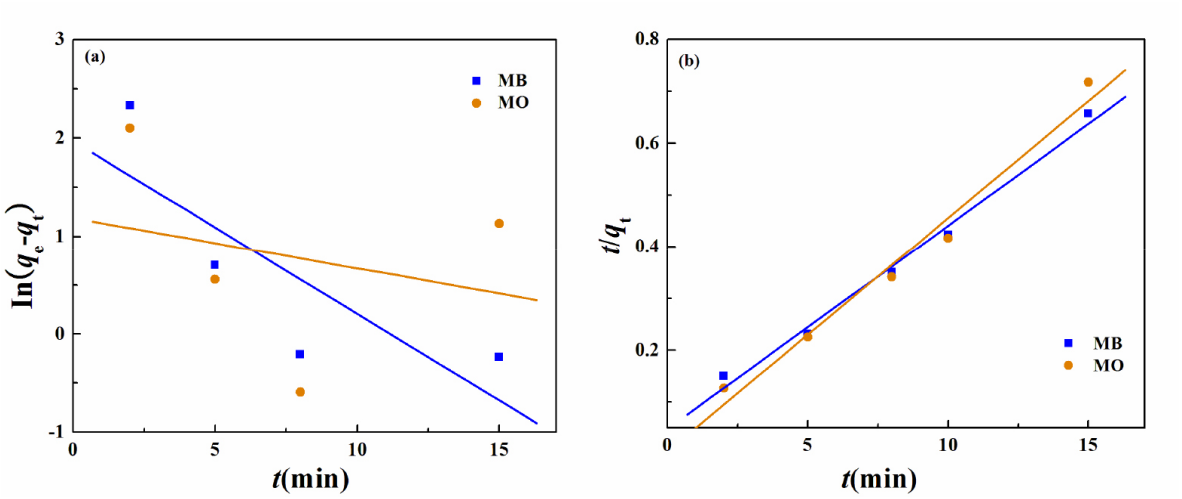

Fig. 7. (a) Pseudo-first-order and (b) pseudo-second-order kinetics fitting curves for MB and MO adsorption onto CCS_1.

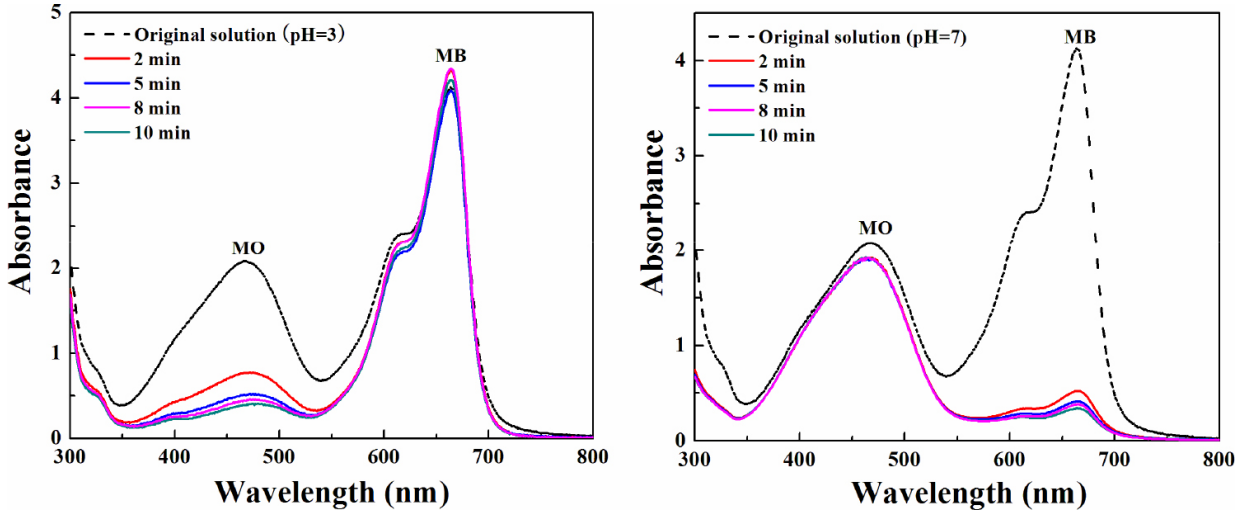

Fig. 8. Selective adsorption performance of CCS_1 in MO/MB binary system.

separated efficiently the cationic and anionic mixed dyes just by adjusting pH of the binary dyes system.

3.5. Possible adsorption mechanism

After adsorption (Fig. 9(a)), a new peak due to C=C stretching of the benzenoid ring of dye was observed at 1,508 or 1,482 cm^{-1} for MO or MB, respectively. The broad band at 3,440 cm^{-1} assigned to –OH and –NH stretching vibrations shifted slightly to 3,445 cm^{-1}. Moreover, the bands at 1,423 and 1,380 cm^{-1} attributed to the symmetric stretching vibration of carboxyl and the primary amine of CS shifted, and the intensity weakened slightly after the dye adsorption, that might due to the interaction between dye molecules and the functional groups of CCS_1 [48,53]. After MB adsorption, the peaks attributed to the stretching vibration of C–N at 1,323 cm^{-1} shifted to 1,334 cm^{-1} and strengthened, indicating the effective adsorption of MB onto CCS_1 adsorbent.

Based on the above discussions, it can be concluded that the electrostatic interactions acted as the main driving force for adsorption of dyes between: (i) the cationic functional groups in MB and negatively charged $–COO^-$ and $–O^-$ in CCS_1 in alkaline conditions ($pH > pH_{zpc}$); (ii) the sulfonate group in MO molecules ($R–SO_3Na$) and the positively charged $–NH_3^+$ and $–OH_2^+$ in acidic conditions ($pH < pH_{zpc}$).

At the same time, covalent bonding was also involved in the adsorption process. At pH_{zpc}, the color removal of 69.53% for MB and 24.32% for MO were obtained, respectively (Fig. 5), indicating that not only electrostatic interactions between adsorbent and MB or MO, but also the hydrogen bonding interactions involved in the adsorption. The hydrogen bonds formed between the OH and NH_2 groups of CCS_1 and N, S atoms in MB and MO owing to the high electronegativity [6].

3.6. Recycle studies

Recyclability is an important factor of adsorbents for their further practical applications. CCS_1 showed different recycle adsorption abilities toward both MO and MB after desorption with ethanol. After desorption, the re-adsorption of MB (Fig. 10(a)) occurred efficiently at alkaline condition (pH = 11), while adsorbed hardly at neutral condition (pH = 7), suggesting that MB desorption was also pH dependent. For MO (Fig. 10(b)), after five adsorption–desorption recycles, MO kept higher removal efficiency (about 87%) at acid condition (pH = 3), indicating that adsorption performance of CCS_1 was excellent and can be recycled facilely for MO, and should have potential application prospects in anionic dye wastewater treatment.

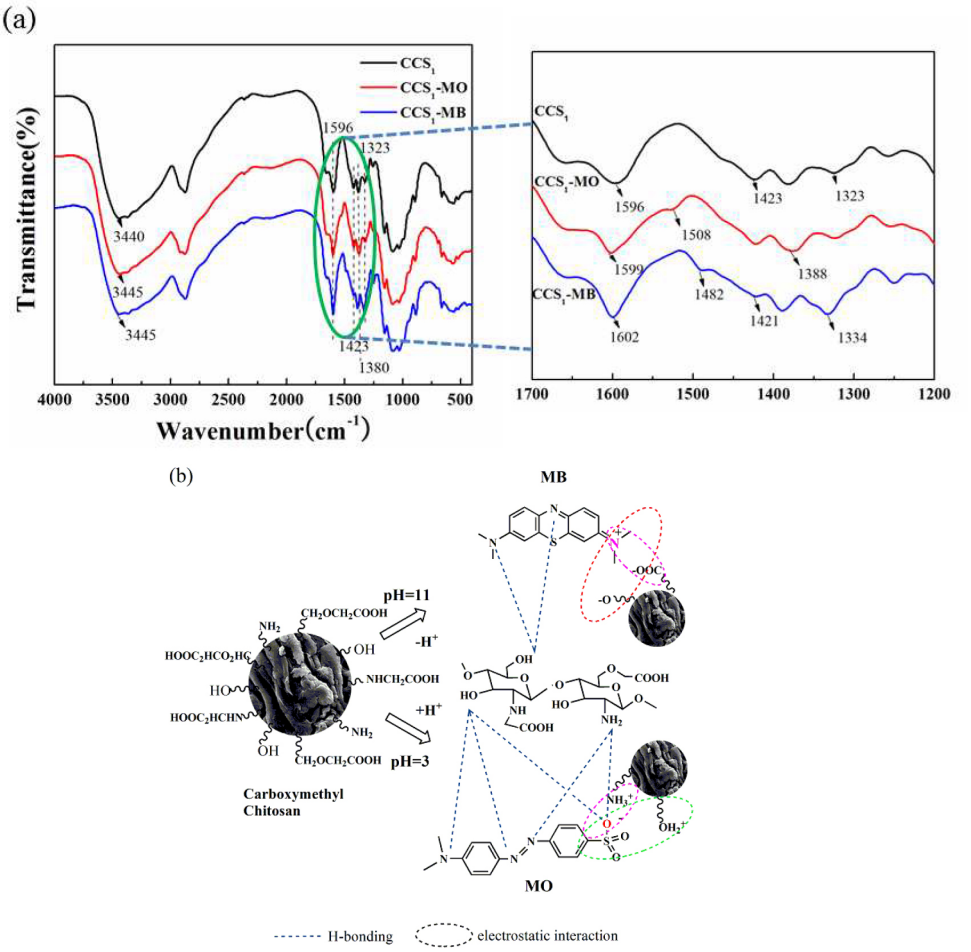

Fig. 9. (a) FT-IR spectra of CCS_1 before and after adsorption and (b) possible adsorption mechanism.

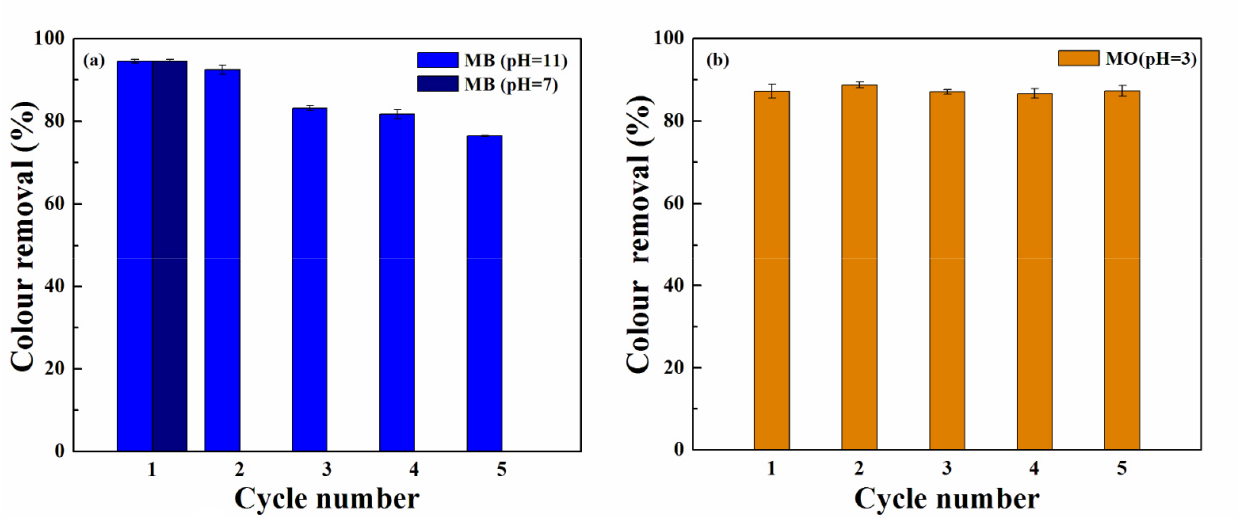

Fig. 10. Recyclability of CCS_1 for MB and MO adsorption.

4. Conclusion

pH-sensitive adsorbents CCS_x with selective and tunable adsorption property in single and binary systems were facilely synthesized and characterized by various techniques. The adsorption of MB was effective at higher MCA dosages (>1:1) and pH values(≥5); while lower MCA amounts(<1:1) and pH values (≤3) enhanced MO adsorption significantly, which was mainly attributed to the functional groups and negative or positive charged properties of the surface of CCS_x adsorbents. A total of 94.5% of MB and 87.2% of MO could be removed by CCS_1 at pH7 and pH3, respectively, within 10 min. The adsorption process fitted better with Langmuir isotherm and pseudo-second-order model and indicating the adsorption was monolayer and chemisorptions dominated the sorption process. Moreover, MB or MO could be adsorbed selectively at pH 7 or 3, and thus separated efficiently from MB/MO binary system just by adjusting pH of the mixture. In one word, CCS_x adsorbents are pH sensitive with tunable adsorption properties which should have great application potentials in textile wastewater treatment.

References

[1] G.L. Dotto, F.K. Rodrigues, E.H. Tanabe, R. Fröhlich, D.A. Bertuol, T.R. Martins, E.L. Foletto, Development of chitosan/bentonite hybrid composite to remove hazardous anionic and cationic dyes from colored effluents, J. Environ. Chem. Eng., 4 (2016) 3230–3239.

[2] J. Qiu, Y. Feng, X. Zhang, M. Jia, J. Yao, Acid-promoted synthesis of UiO-66 for highly selective adsorption of anionic dyes: adsorption performance and mechanisms, J. Colloid Interface Sci., 499 (2017) 151–158.

[3] M. Martínez-Quiroz, E.A. López-Maldonado, A. Ochoa-Terán, M.T. Oropeza-Guzman, G.E. Pina-Luis, J. Zeferino-Ramírez, Innovative uses of carbamoyl benzoic acids in coagulation-flocculation's processes of wastewater, Chem. Eng. J., 307 (2017) 981–988.

[4] A. Sharma, G. Sharma, M. Naushad, A.A. Ghfar, D. Pathania, Remediation of anionic dye from aqueous system using bio-adsorbent prepared by microwave activation, Environ. Technol., 39 (2018) 917–930.

[5] E. Daneshvar, A. Vazirzadeh, A. Niazi, M. Kousha, M. Naushad, A. Bhatnagar, Desorption of methylene blue dye from brown macroalga: effects of operating parameters, isotherm study and kinetic modeling, J. Cleaner Prod., 152 (2017) 443–453.

[6] A.B. Albadarin, M.N. Collins, M. Naushad, S. Shirazian, G. Walker, C. Mangwandi, Activated lignin-chitosan extruded blends for efficient adsorption of methylene blue, Chem. Eng. J., 307 (2017) 264–272.

[7] A.A. Alqadami, M. Naushad, M.A. Abdalla, M.R. Khan, Z.A. Alothman, Adsorptive removal of toxic dye using Fe_3O_4–TSC nanocomposite: equilibrium, kinetic, and thermodynamic studies, J. Chem. Eng. Data, 61 (2016) 3806–3813.

[8] D. Pathania, R. Katwal, G. Sharma, M. Naushad, M.R. Khan, A.H. Al-Muhtaseb, Novel guar gum/Al_2O_3 nanocomposite as an effective photocatalyst for the degradation of malachite green dye, Int. J. Biol. Macromol., 87 (2016) 366–374.

[9] D. Pathania, G. Sharma, A. Kumar, M. Naushad, S. Kalia, A. Sharma, Z.A. ALOthman, Combined sorptional-photocatalytic remediation of dyes by polyaniline Zr(IV) selenotungstophosphate nanocomposite, Toxicol. Environ. Chem., 97 (2015) 526–537.

[10] M. Naushad, Z.A. Alothman, M.R. Awual, S.M. Alfadul, T. Ahamad, Adsorption of rose bengal dye from aqueous solution by amberlite Ira-938 resin: kinetics, isotherms, and thermodynamic studies, Desal. Wat. Treat., 57 (2016) 13527–13533.

[11] S. Ming-Twang, M.A.A. Zaini, L.M. Salleh, M.A.C. Yunus, M. Naushad, Potassium hydroxide-treated palm kernel shell sorbents for the efficient removal of methyl violet dye, Desal. Wat. Treat., 84 (2017) 262–270.

[12] A. Kumar, C. Guo, G. Sharma, D. Pathania, M. Naushad, S. Kalia, P. Dhiman, Magnetically recoverable ZrO_2/Fe_3O_4/chitosan nanomaterials for enhanced sunlight driven photoreduction of carcinogenic Cr(vi) and dechlorination and mineralization of 4-chlorophenol from simulated waste water, RSC Adv., 6 (2016) 13251–13263.

[13] M. Curcio, L. Diaz-Gomez, G. Cirillo, A. Concheiro, F. Iemma, C. Alvarez-Lorenzo, pH/redox dual-sensitive dextran nanogels for enhanced intracellular drug delivery, Eur. J. Pharm. Biopharm., 117 (2017) 324–332.

[14] M. Martínez-Quiroz, E.A. López-Maldonado, A. Ochoa-Terán, G.E. Pina-Luis, M.T. Oropeza-Guzman, Modification of chitosan with carbamoyl benzoic acids for testing its coagulant-flocculant and binding capacities in removal of metallic ions typically contained in plating wastewater, Chem. Eng. J., 332 (2018) 749–756.

[15] H. Tang, W. Zhou, L. Zhang, Adsorption isotherms and kinetics studies of malachite green on chitin hydrogels, J. Hazard. Mater., 209–210 (2012) 218–225.

[16] P. Kanmani, J. Aravind, M. Kamaraj, P. Sureshbabu, S. Karthikeyan, Environmental applications of chitosan and

cellulosic biopolymers: a comprehensive outlook, Bioresour. Technol., 242 (2017) 295–303.
[17] V.M. Esquerdo, T.R.S. Cadaval Jr., G.L. Dotto, L.A.A. Pinto, Chitosan scaffold as an alternative adsorbent for the removal of hazardous food dyes from aqueous solutions, J. Colloid Interface Sci., 424 (2014) 7–15.
[18] L. Hu, P. Zhang, X. Wang, X. Cheng, J. Qin, R. Tang, pH-sensitive carboxymethyl chitosan hydrogels via acid-labile ortho ester linkage for potential biomedical applications, Carbohydr. Polym., 178 (2017) 166–179.
[19] X. Xu, B. Bai, H. Wang, Y. Suo, Synthesis of human hair fiber-impregnated chitosan beads functionalized with citric acid for the adsorption of lysozyme, RSC Adv., 7 (2017) 6636–6647.
[20] H.C. Yang, J.L. Gong, G.M. Zeng, P. Zhang, J. Zhang, H.Y. Liu, S.Y. Huan, Polyurethane foam membranes filled with humic acid-chitosan crosslinked gels for selective and simultaneous removal of dyes, J. Colloid Interface Sci., 505 (2017) 67–78.
[21] H.R. Kim, J.W. Jang, J.W. Park, Carboxymethyl chitosan-modified magnetic-cored dendrimer as an amphoteric adsorbent, J. Hazard. Mater., 317 (2016) 608–616.
[22] M. Zheng, B. Han, Y. Yang, W. Liu, Synthesis, characterization and biological safety of O-carboxymethyl chitosan used to treat Sarcoma 180 tumor, Carbohydr. Polym., 86 (2011) 231–238.
[23] X. Jiang, L. Chen, W. Zhong, A new linear potentiometric titration method for the determination of deacetylation degree of chitosan, Carbohydr. Polym., 54 (2003) 457–463.
[24] M.W. Sabaa, H.M. Abdallah, N.A. Mohamed, R.R. Mohamed, Synthesis, characterization and application of biodegradable crosslinked carboxymethyl chitosan/poly(vinyl alcohol) clay nanocomposites, Mater. Sci. Eng., C, 56 (2015) 363–373.
[25] G. Sharma, M. Naushad, A.H. Al-Muhtaseb, A. Kumar, M.R. Khan, S. Kalia, Shweta, M. Bala, A. Sharma, Fabrication and characterization of chitosan-crosslinked-poly(alginic acid) nanohydrogel for adsorptive removal of Cr(VI) metal ion from aqueous medium, Int. J. Biol. Macromol., 95 (2017) 484–493.
[26] D. Pathania, D. Gupta, A.H. Al-Muhtaseb, G. Sharma, A. Kumar, M. Naushad, T. Ahamad, S.M. Alshehri, Photocatalytic degradation of highly toxic dyes using chitosan-g-poly(acrylamide)/ZnS in presence of solar irradiation, J. Photochem. Photobiol., A, 329 (2016) 61–68.
[27] X.G. Chen, H.J. Park, Chemical characteristics of O-carboxymethyl chitosans related to the preparation conditions, Carbohydr. Polym., 53 (2003) 355–359.
[28] B. Doshi, E. Repo, J.P. Heiskanen, J.A. Sirviö, M. Sillanpää, Effectiveness of N,O-carboxymethyl chitosan on destabilization of Marine Diesel, Diesel and Marine-2T oil for oil spill treatment, Carbohydr. Polym., 167 (2017) 326–336.
[29] M. Abbasi, Synthesis and characterization of magnetic nanocomposite of chitosan/SiO_2/carbon nanotubes and its application for dyes removal, J. Cleaner Prod., 145 (2017) 105–113.
[30] S.E. Subramani, N. Thinakaran, Isotherm, kinetic and thermodynamic studies on the adsorption behaviour of textile dyes onto chitosan, Process Saf. Environ. Prot, 106 (2017) 1–10.
[31] T.R.A. Sobahi, M.Y. Abdelaal, M.S.I. Makki, Chemical modification of Chitosan for metal ion removal, Arabian J. Chem., 7 (2014) 741–746.
[32] K. Liu, L. Chen, L. Huang, Y. Lai, Evaluation of ethylenediamine-modified nanofibrillated cellulose/chitosan composites on adsorption of cationic and anionic dyes from aqueous solution, Carbohydr. Polym., 151 (2016) 1115–1119.
[33] K. Gul, S. Sohni, M. Waqar, F. Ahmad, N.A. Nik Norulaini, A.K. Mohd. Omar, Functionalization of magnetic chitosan with graphene oxide for removal of cationic and anionic dyes from aqueous solution, Carbohydr. Polym., 152 (2016) 520–531.
[34] S. Sun, A. Wang, Adsorption kinetics of Cu(II) ions using N,O-carboxymethyl-chitosan, J. Hazard. Mater., 131 (2006) 103–111.
[35] N.H. Elsayed, M. Monier, I. Youssef, Fabrication of photo-active trans-3-(4-pyridyl) acrylic acid modified chitosan, Carbohydr. Polym., 172 (2017) 1–10.
[36] M. Monier, Y. Wei, A.A. Sarhan, D.M. Ayad, Synthesis and characterization of photo-crosslinkable hydrogel membranes based on modified chitosan, Polymer, 51 (2010) 1002–1009.
[37] Y. Cao, Y. Ding, L. Zhang, G. Shi, X. Sang, C. Ni, Preparation of surface-modified, micrometer-sized carboxymethyl chitosan drug-loaded microspheres, J. Appl. Polym. Sci., 135 (2018) 45731.
[38] Z. Yu, Q. Dang, C. Liu, D. Cha, H. Zhang, W. Zhu, Q. Zhang, B. Fan, Preparation and characterization of poly(maleic acid)-grafted cross-linked chitosan microspheres for Cd(II) adsorption, Carbohydr. Polym., 172 (2017) 28–39.
[39] O. Molatlhegi, L. Alagha, Adsorption characteristics of chitosan grafted copolymer on kaolin, Appl. Clay Sci., 150 (2017) 342–353.
[40] Y. Huang, J. Huang, J. Cai, W. Lin, Q. Lin, F. Wu, J. Luo, Carboxymethyl chitosan/clay nanocomposites and their copper complexes: fabrication and property, Carbohydr. Polym., 134 (2015) 390–397.
[41] S. Srivastava, S.B. Agrawal, M.K. Mondal, Synthesis, characterization and application of *Lagerstroemia speciosa* embedded magnetic nanoparticle for Cr (VI) adsorption from aqueous solution, J. Environ. Sci., 55 (2017) 283–293.
[42] D. Xu, W. Li, K. Wang, Y. Bai, Q. Lin, M. Gao, H. Ma, Hydroxy-aluminium and cetyltrimethyl ammonium bromide modified bentonite as adsorbent and its adsorption for Orange II, Desal. Wat. Treat., 94 (2017) 244–253.
[43] Q. Lin, M. Gao, J. Chang, H. Ma, Adsorption properties of crosslinking carboxymethyl cellulose grafting dimethyl-diallylammonium chloride for cationic and anionic dyes, Carbohydr. Polym., 151 (2016) 283–294.
[44] L. Obeid, A. Bée, D. Talbot, S. Ben Jaafar, V. Dupuis, S. Abramson, V. Cabuil, M. Welschbillig, Chitosan/maghemite composite: a magsorbent for the adsorption of methyl orange, J. Colloid Interface Sci., 410 (2013) 52–58.
[45] L. Zeng, M. Xie, Q. Zhang, Y. Kang, X. Guo, H. Xiao, Y. Peng, J. Luo, Chitosan/organic rectorite composite for the magnetic uptake of methylene blue and methyl orange, Carbohydr. Polym., 123 (2015) 89–98.
[46] L. Liu, Z.Y. Gao, X.P. Su, X. Chen, L. Jiang, J.M. Yao, Adsorption removal of dyes from single and binary solutions using a cellulose-based bioadsorbent, ACS Sustainable Chem Eng., 3 (2015) 432–442.
[47] Y. Wang, X. Liu, H. Wang, G. Xia, W. Huang, R. Song, Microporous spongy chitosan monoliths doped with graphene oxide as highly effective adsorbent for methyl orange and copper nitrate ($Cu(NO_3)_2$) ions, J. Colloid Interface Sci., 416 (2014) 243–251.
[48] W. Li, P. Zuo, D. Xu, Y. Xu, K. Wang, Y. Bai, H. Ma, Tunable adsorption properties of bentonite/carboxymethyl cellulose-g-poly(2-(dimethylamino) ethylmethacrylate) composites toward anionic dyes, Chem. Eng. Res. Des., 124 (2017) 260–270.
[49] E.F. Lessa, M.S. Gularte, E.S. Garcia, A.R. Fajardo, Orange waste: a valuable carbohydrate source for the development of beads with enhanced adsorption properties for cationic dyes, Carbohydr. Polym., 157 (2017) 660–668.
[50] G. Wang, S. Wang, W. Sun, Z. Sun, S. Zheng, Oxygen functionalized carbon nanocomposite derived from natural illite as adsorbent for removal of cationic and anionic dyes, Adv. Powder Technol., 28 (2017) 1943–1953.
[51] B.J. Yao, W.L. Jiang, Y. Dong, Z.X. Liu, Y.B. Dong, Post-synthetic polymerization of UiO-66-NH_2 nanoparticles and polyurethane oligomer toward stand-alone membranes for dye removal and separation, Chem. Eur. J., 22 (2016) 10565–10571.
[52] H. Li, X. Cao, C. Zhang, Q. Yu, Z. Zhao, X. Niu, X. Sun, Y. Liu, L. Ma, Z. Li, Enhanced adsorptive removal of anionic and cationic dyes from single or mixed dye solutions using MOF PCN-222†, RSC Adv., 7 (2017) 16273–16281.
[53] W. Li, D. Xu, M. Gao, Q. Lin, H. Ma, Adsorption studies of Orange II onto polyaniline/bentonite nanocomposite, Water Sci. Technol., 76 (2017) 337–354.